Molecular dissection of the Erv41-Erv46 retrograde receptor reveals a conserved cysteine-rich region in Erv46 required for retrieval activity

Kristofer J. Keiser and Charles Barlowe*
Department of Biochemistry and Cell Biology, Geisel School of Medicine at Dartmouth, Hanover, NH 03755

ABSTRACT **The Erv41-Erv46 complex is a conserved retrograde cargo receptor that retrieves ER resident proteins from Golgi compartments in a pH-dependent manner. Here we functionally dissect the Erv46 subunit and define an approximately 60 residue cysteine-rich region that is unique to the Erv46 family of proteins. This cysteine-rich region contains two vicinal cysteine pairs in CXXC and CCXXC configurations that are each required for retrieval activity in cells. Mutation of the individual cysteine residues produced stable Erv46 proteins that were partially reduced and form mixed-disulfide species on nonreducing gels. Conserved hydrophobic amino acids within the cysteine-rich region of Erv46 were also required for retrieval function in cells. In vitro binding experiments showed that this hydrophobic patch is required for direct cargo binding. Surprisingly, the Erv46 cysteine mutants continued to bind cargo in cell-free assays and produced an increased level of Erv46-cargo complexes in cell extracts suggesting that disulfide linkages in the cysteine-rich region perform a role in releasing bound cargo. On the basis of these findings, we propose that both pH and redox environments regulate cargo binding to a hydrophobic site within the cysteine-rich region of Erv46.**

Monitoring Editor
Akihiko Nakano
RIKEN

Received: Sep 3, 2019
Revised: Nov 21, 2019
Accepted: Dec 6, 2019

INTRODUCTION

Nascent secretory proteins are folded and packaged into COPII carriers at the endoplasmic reticulum (ER) for anterograde transport to the Golgi complex. To balance forward transport, a COPI-dependent retrograde pathway returns membrane lipids, transport machinery, and escaped ER resident proteins from Golgi compartments back to the ER (Barlowe and Helenius, 2016). Despite this general framework, there is no coherent understanding of how diverse biosynthetic cargo molecules advance while organelles retain their constituent proteins in the face of dynamic bidirectional traffic. Context-dependent recognition of cytoplasmically exposed sorting signals by the COPI complex (Jackson *et al.*, 2012; Ma and Goldberg, 2013) and COPII coat complex (Miller *et al.*, 2003; Mancias and Goldberg, 2007) efficiently capture certain transmembrane proteins into transport carriers. In addition, transmembrane cargo receptors link luminal cargo to these coat complexes through binding reactions that can be regulated by pH gradients (Wilson *et al.*, 1993), calcium concentration (Appenzeller-Herzog *et al.*, 2004), and redox environment (Yang *et al.*, 2016). However, our mechanistic insight on reversible cargo binding by receptors is limited. We recently identified Erv41-Erv46 complex as a new retrograde sorting receptor that retrieves non–KDEL-bearing ER-resident proteins (Shibuya *et al.*, 2015). In this report, we define the molecular elements of Erv41-Erv46 complex that are necessary and sufficient for cargo binding and retrieval.

Erv41 and Erv46 were initially detected in proteomic analyses of COPII vesicles and these two proteins are highly conserved in nature (Otte *et al.*, 2001). The mammalian orthologues, known as ERGIC2

This article was published online ahead of print in MBoC in Press (http://www.molbiolcell.org/cgi/doi/10.1091/mbc.E19-08-0484) on December 11, 2019.

*Address correspondence to: Charles Barlowe (charles.barlowe@dartmouth.edu).

Abbreviations used: co-IP, coimmunoprecipitation; CV, column volume; DTT, dithiothreitol; ER, endoplasmic reticulum; NEM, N-ethylmaleimide; PBS, phosphate-buffered saline; PEG-Mal, PEG-maleimide; TBS, Tris-buffered saline.

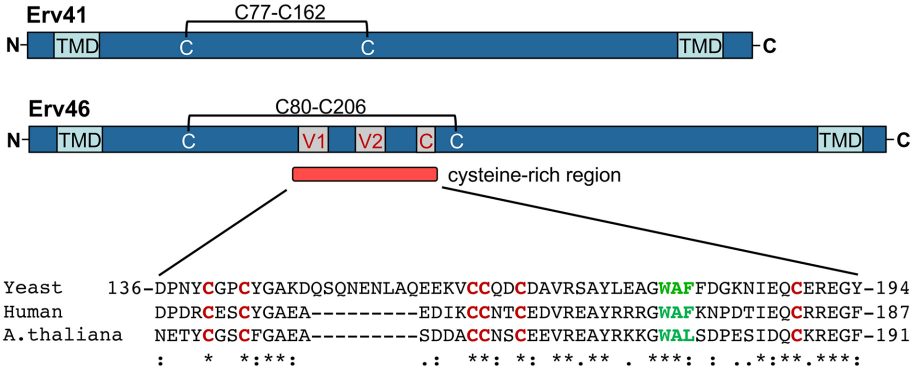

FIGURE 1: Schematic showing features of the Erv41 and Erv46 proteins. The proteins share overall sequence identity (28%) with two transmembrane domains (TMD), large luminal domains that contain structural disulfide bonds, and cytoplasmic C-terminal sorting signals. Erv46 and related family members contain an approximately 60 amino acid cysteine-rich region with two vicinal cysteine pairs and a total of six invariant cysteine residues shown in red. A conserved hydrophobic stretch of amino acids is highlighted in green. Yeast Erv46 (P39727), human ERGIC3 (Q9Y282), and Arabidopsis thaliana ERV-A (Q9LM16) sequences were aligned with Clustal Omega.

and ERIGIC3, also appear to operate in Golgi to ER retrograde transport and are required for Ricin and Shiga intoxication (Moreau *et al.*, 2011; Adolf *et al.*, 2019). The Erv41 and Erv46 proteins are related and each contain two transmembrane segments with a topology that places short N- and C-termini in the cytoplasm with most of the protein luminally oriented. The C-terminus of Erv41 contains hydrophobic residues required for binding to COPII subunits and for ER export, whereas the C-terminus of Erv46 contains a COPI binding di-lysine motif that is required for retrograde transport from the Golgi (Otte and Barlowe, 2002). Erv41-Erv46 forms an obligate hetero-oligomer that is required for protein stability and dynamic cycling of this complex between the ER and the Golgi compartments. Deletion of either subunit results in a failure to retain specific ER resident proteins (Shibuya *et al.*, 2015). Erv41-Erv46 binds specific ER resident cargo in a pH-dependent manner such that binding is promoted at a mildly acidic pH of early Golgi compartments (Shibuya *et al.*, 2015).

The Erv41 and Erv46 proteins share significant overall sequence identity (28%) as do their mammalian counterparts ERGIC2 and ERGIC3 (38%). A crystal structure of the luminal domain of yeast Erv41 has been determined to 2.0 Å (Biterova *et al.*, 2013). The core structure or Erv41 consists of a twisted β-sandwich with no significant structural homology to other known proteins. Erv41 also contains a single structural disulfide bond between residues C77 and C162, which is an invariant feature across Erv41 and Erv46 family members. However, a distinguishing feature between the Erv41 and Erv46 family of proteins can be attributed to insertion of an approximately 60 amino acid cysteine-rich sequence near the middle of the Erv46 protein (Figure 1). Modeling based on the Erv41 structure (Biterova *et al.*, 2013), places the Erv46 cysteine-rich sequence in a membrane distal region that may permit interaction with luminal cargo. Furthermore, the presence of two highly conserved vicinal dithiols in this cysteine-rich region indicates the potential for redox regulation. Here we investigated the role of these cysteine residues in addition to other conserved hydrophobic residues in this region of Erv46. Our findings indicate a critical function for these elements in Erv41-Erv46 cargo binding and retrieval function.

RESULTS

Erv46 contains two conserved vicinal CXXC motifs

To dissect the interaction mechanism between the Erv41-Erv46 complex and cargo, the primary amino acid sequence of Erv46 was analyzed with HHpred (Zimmermann *et al.*, 2018) and NCBI-BLAST. The HHpred program indicated that the cysteine-rich region of Erv46 contains a potential thioredoxin-like domain aligning with protein disulfide isomerases and glutaredoxins (Figure 1). Although this cysteine-rich region has been previously recognized (Otte *et al.*, 2001), it had not been characterized as having potential thioredoxin-like features. Erv46 was then compared with other sequences by NCBI-BLAST and the vicinal CXXC motifs within the cysteine-rich region are highly conserved, further suggesting this region may contain thioredoxin-like properties. There is some variation in the intervening residues and not all elements of the thioredoxin fold are present in Erv46. However, all Erv46 family members contain a pair of vicinal dithiols with two additional cysteine residues adjacent to, and 23 residues C-terminal to, the second vicinal dithiol, for a total of six conserved cysteines within this region (Figure 1). Notably, Erv41 lacks this cysteine-rich region but does contain two conserved cysteine residues that bracket the insertion and form a structural disulfide bond (Biterova *et al.*, 2013). Sequence alignments indicate the structural disulfide is conserved in Erv46 and we find below that the C80 and C206 residues are critical for Erv46 stability. Finally, Erv46 contains single cysteine residues within each transmembrane domain. However, we observe that mutation of the transmembrane domain cysteine residues (C33 and C384) does not produce detectable changes in Erv46 function as described below.

Mutation of cysteine-rich region cysteines influences Erv46 function

We investigated the role of these six conserved cysteine residues in Erv46 through site-directed mutagenesis. Single cysteine to serine mutation of each residue resulted in a loss of retrieval activity as measured by decreases in cellular levels of Gls1 (Figure 2A), which is due to mislocalization and degradation of Gls1 (Shibuya *et al.*, 2015). The level of Gls1 in each mutant was reduced to an equivalent level as the *erv46*Δ strain (Figure 2B) indicating that the mutations caused a complete loss of function. Importantly, the cysteine to serine point mutations resulted in normal expression of Erv46 (Figure 2A), suggesting that the mutant proteins are not misfolded. Moreover, in subsequent experiments, we observed that these Erv46 C/S mutants assemble into stable complexes with Erv41 and cycle between the ER and the Golgi complex. However, examination of the Erv46 C/S mutants on nonreducing PAGE revealed prominent changes in the mobility pattern of Erv46 (Figure 2C). For these experiments, cells were lysed in the presence of 10 mM N-ethylmaleimide (NEM) to cap free cysteines prior to running nonreducing gels. First, we note that under nonreducing conditions, most wild-type Erv46 protein run as an oxidized species just below the 45 kDa molecular weight marker. In contrast, all six of the cysteine to serine mutants are shifted to a slower migrating form above the 45 kDa marker with a corresponding loss of oxidized Erv46.

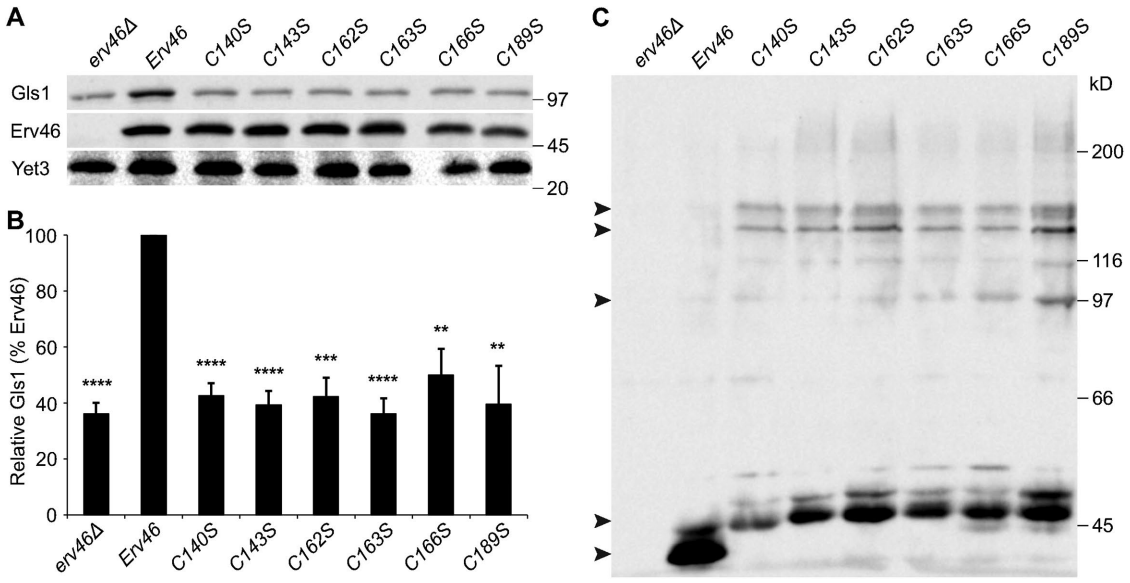

FIGURE 2: Erv46 cysteine to serine mutants decrease Gls1 retrieval and alter Erv46 migration on nonreducing PAGE. (A) Immunoblot and (B) quantification of Gls1 levels ($n = 3$) from whole cell extracts of an *erv46Δ* strain (CBY799) expressing wild-type or indicated Erv46 mutants from pRS316-Erv46 *CEN* based plasmids. Gls1 was normalized to Yet3 as the loading control and plotted as a percentage relative to wild type. Error bars represent SEM and one-way analysis of variance (ANOVA) used to compare each mutant to wild type with p values of: ****$p < 0.0001$; ***$p < 0.001$; **$p < 0.01$. (C) Semi-intact cells of the same strains in A were lysed in the presence of NEM, resolved by nonreducing SDS–PAGE, and immunoblotted for Erv46. Arrowheads from the bottom up indicate oxidized, partially reduced, and mixed disulfide forms of Erv46.

Strikingly, the Erv46 C/S mutants also formed high molecular weight species ranging in sizes from 95 kDa to more than 200 kDa. These higher molecular weight forms are likely the result of mixed-disulfide species that form when unpaired cysteine residues in Erv46 react with other proteins (Holmgren, 1985; Gilbert, 1990). The level of trapped disulfide-bonded intermediates varies between different cysteine mutants (e.g., increased in C162S and C189S) although the overall pattern is similar. In darker exposures (Supplemental Figure S1), we also detected some similar species with wild-type Erv46 suggesting that these could be intermediates in the normal Erv46 retrieval cycle. We note that the known cargo proteins, Gls1 and Fpr2, could not be detected in these higher molecular weight species by immunoblot.

To determine the level of free cysteines in Erv46 and in mutant forms of Erv46, we conducted experiments using PEG-Maleimide 5k (PEG-Mal), which produces an approximate 5 kDa shift for each reactive cysteine residue. Semi-intact cells expressing the indicated Erv46 proteins were analyzed on standard reducing PAGE (Figure 3A) or lysed in the presence of trichloroacetic acid to block redox reactions and to precipitate proteins. Protein pellets were resuspended in buffer (pH = 7.5) containing PEG-Mal and SDS detergent and then resolved on reducing gels for Erv46 immunoblot (Figure 3B). For wild-type Erv46, we detected a 10 kDa increase in size indicating the presence of two free cysteine residues. However, treatment of each of the single Erv46 C/S mutants resulted in a higher molecular weight smear indicative of heterogeneity in the number of reactive-free cysteine residues. Removing additional cysteine residues from the cysteine-rich region simplified the pattern with conversion of all six cysteine residues to serines producing the initial 10 kDa shift (Figure 3B). Finally, mutation of the transmembrane domain cysteine residues, C33A and C384A, in an otherwise wild-type Erv46 protein, produced a protein that was unmodified by PEG-Mal (Figure 3C). This finding indicates that the 10 kDa increase in size is caused by reactivity of the two transmembrane domain cysteines with PEG-Mal. Mutation of these transmembrane cysteines does not produce detectable changes in the stability and function of Erv46 (Supplemental Figure S2). Moreover, these results show that the six cysteine residues in the cysteine-rich region of wild-type Erv46 are predominantly in disulfide linkages under normal growth conditions.

Erv46 cysteine-rich region mutations permit assembly and trafficking of the Erv41-Erv46 complex

Mutations that delete or destabilize Erv46 cause mislocalization and turnover of the coassociated Erv41 subunit (Otte and Barlowe, 2002). Therefore, we tested whether the Erv46 cysteine-rich region mutations interfered with Erv41-Erv46 assembly and trafficking. For comparisons, we examined the Erv46ΔC mutant, which lacks an ER export signal, and the Erv46 C80A mutant, which is predicted to disrupt a structural disulfide bond in Erv46 and destabilize the protein. As shown in Figure 4, we can monitor expression levels by immunoblot and trafficking between the ER (P13) and Golgi (P100) membranes by differential centrifugation of gently lysed yeast cells (Otte and Barlowe, 2002). In the *erv46Δ* strain, we observed that Erv41 was strongly destabilized as previously reported (Otte *et al.*, 2001). When the *erv46Δ* strain expresses plasmid-borne Erv46, the Erv41 subunit was stabilized and the Erv41-Erv46 complex was detected in both ER (P13) and Golgi (P100) fractions. Expression of Erv46ΔC stabilized Erv41; however, the assembled Erv41-Erv46ΔC complex was shifted to the ER (P13) fraction (Otte *et al.*, 2001). Expression of Erv46 C80A structural mutant caused reduced levels of both Erv46 and Erv41 with residual levels of Erv46 shifted to the ER (P13) fraction as would be expected for a terminally misfolded version of Erv46. Finally, expression of Erv46 C143S stabilizes Erv41 and this Erv41-Erv46 C143S complex was distributed between ER and Golgi fractions indicative of normal trafficking. We similarly find

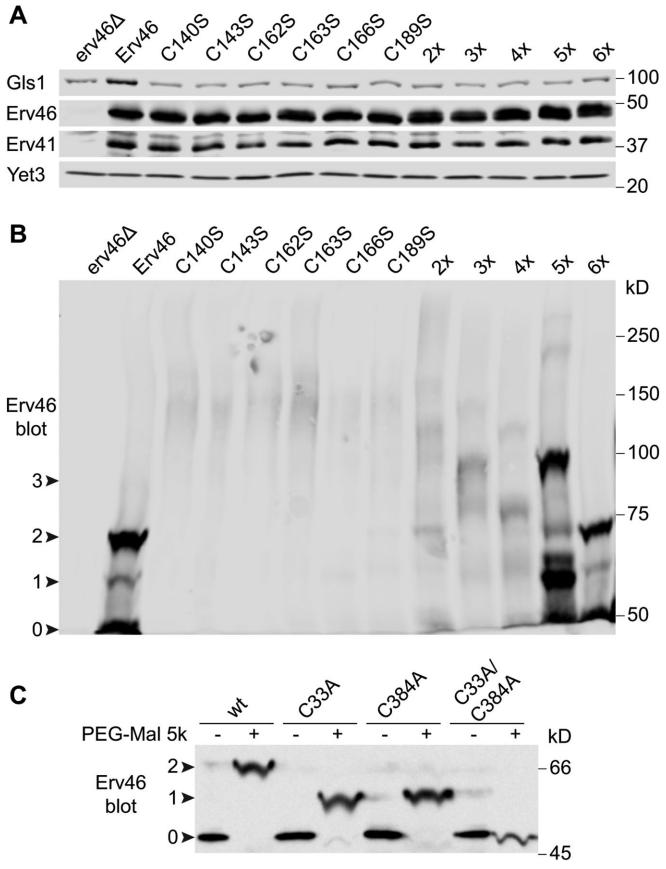

FIGURE 3: Determining free thiols in Erv46 and cysteine mutants by PEGylation. (A) Wild-type Erv46 and the indicated C/S mutants were expressed from pRS316 in an *erv46Δ* strain (CBY799) and analyzed by immunoblot to monitor Erv46 stability, complex assembly with Erv41, and Gls1 retrieval activity. Yet3 served as a loading control. For Erv46 proteins containing multiple C/S mutations: 2× = C140S/C163S; 3× = C140S/C143S/C163S; 4× = C140S/C143S/C163S/166S; 5× = C140S/C143S/C162S/C163S/C166S; 6× = C140S/C143S/C162S/C163S/C166S/C189S. (B) Wild-type and Erv46 mutant proteins were treated with PEG-Mal 5K, resolved by 7.5% SDS–PAGE and detected by Erv46 immunoblot. Unlabelled Erv46 runs at the bottom of the gel and PEGylated Erv46 migrates in higher molecular weight ranges. Unmodified, single, double and triple PEGylated forms of Erv46 are indicted by arrowheads. (C) Erv46 immunoblot from PEGylation reactions of cysteine mutants demonstrates that the primary PEGylation sites in wild-type Erv46 are the transmembrane domain cysteine residues C33 and C384.

that the Erv46 C163S mutant is distributed between ER and Golgi fractions (Supplemental Figure S3) and that Erv41 was stably expressed in all six C/S mutants in the cysteine-rich region (Figure 3A). On the basis of these results, we conclude that mutations in the cysteine-rich region of Erv46 permit normal assembly and trafficking of the Erv41-Erv46 complex, although cargo retrieval by the complex is uncoupled from its ER–Golgi transport cycle.

Hydrophobic residues within the Erv46 cysteine-rich region are required for Erv46 function

Conserved hydrophobic amino acid residues surrounding an invariant tryptophan 178 were mutated to alanines to determine the impact on Erv46 retrieval activity. The W178A, F180A, and F181A mutants all resulted in stable expression of Erv46 (Figure 5A) that assembled into complexes with Erv41 and trafficked between the ER and the Golgi compartments (Figure 4 and Supplemental Figure S3). These hydrophobic mutants also migrated as oxidized wild-type Erv46 protein on nonreducing PAGE (Supplemental Figure S4) indicating a normal disulfide configuration. However, the W178A mutant displayed partial loss of function in retrieval of Gls1 and Fpr2, whereas the F180A and F181A mutants displayed complete loss of retrieval activity (Figure 5, B and C). It is noteworthy that the W178A mutation produced a greater percentage decrease in Fpr2 levels than in Gls2 levels, suggesting there might be some specificity in cargo binding. On the basis of these findings, we hypothesize that this hydrophobic patch is important for binding to escaped ER resident proteins and directly investigate this possibility in cell-free binding assays described below.

Testing additional conserved residues for function in Erv46 retrieval activity

Other conserved amino acid residues in the cysteine-rich region of Erv46 were tested for influence on retrieval activity, including E158A, Y173A, and E192A. These single point mutations did not display detectable alterations. The thioredoxin superfamily of proteins often utilize an arginine residue downstream of the active vicinal cysteine pair that lowers the pKa of the reactive cysteines to stabilize formation of a thiolate during reoxidation (Lappi *et al.*, 2004; Tian *et al.*, 2006). Therefore, the R191A and R216A mutants were also generated for analysis. Of these two arginine residue mutants, R216A displayed a strong reduction in Fpr2 levels and a more modest reduction in Gls1 levels (Figure 6, A, C, and E) indicating a partial loss of function. However, when the charge inverted mutant R216E was assessed, both Fpr2 and Gls1 were reduced to *erv46Δ* levels (Figure 6, A and E). The R216A mutant contrasts mutations in vicinal cysteine residues (C140S and C163S) and the structural disulfide bond mutants (C80A and C206A) where complete loss of function in retrieval of both Gls1 and Fpr2 was observed (Figure 6B). We also find that that the R216 mutants are stably expressed, display normal migration on nonreducing PAGE, and assemble into complexes with Erv41, indicating minimal effects on protein folding and overall structure (Figure 6A and Supplemental Figure S4). The residues flanking R216 are also conserved; however, mutations in these residues (I214A, N215A, I217A) did not result in any detectable phenotypic changes. As suggested for the hydrophobic residue mutants characterized above, we propose that the R216A and R216E mutants differentially impact binding of cargo to the Erv41-Erv46 complex for subsequent retrieval to the ER. However, it remains to be determined whether R216 plays a role in regulating the pKa of residues in the cysteine-rich region.

Additional mutations were introduced into other conserved amino acid residues in Erv46 and Erv41 to test for function (Supplemental Table S1). Histidine residues are well documented to regulate pH-dependent activity in proteins (Bartlett *et al.*, 2002). Therefore, all eight of the conserved histidine residues in the luminal domain of Erv46 were individually mutated with no direct influence on Gls1 retrieval activity. Erv41 contains a conserved pair of phenylalanines (F145, F146) that align with the hydrophobic WAFF sequence in Erv46. Conversion of these residues in Erv41 to alanines did not produce detectable phenotypes. Similarly, mutation of R172 in Erv41, which aligns with R216 in Erv46, was without effect. However, mutation of the structural cysteine residues in Erv41 (C77, C162) destabilized the protein and produced a complete loss of function in keeping with a critical role for stable assembly of the Erv41-Erv46 complex in retrieval activity.

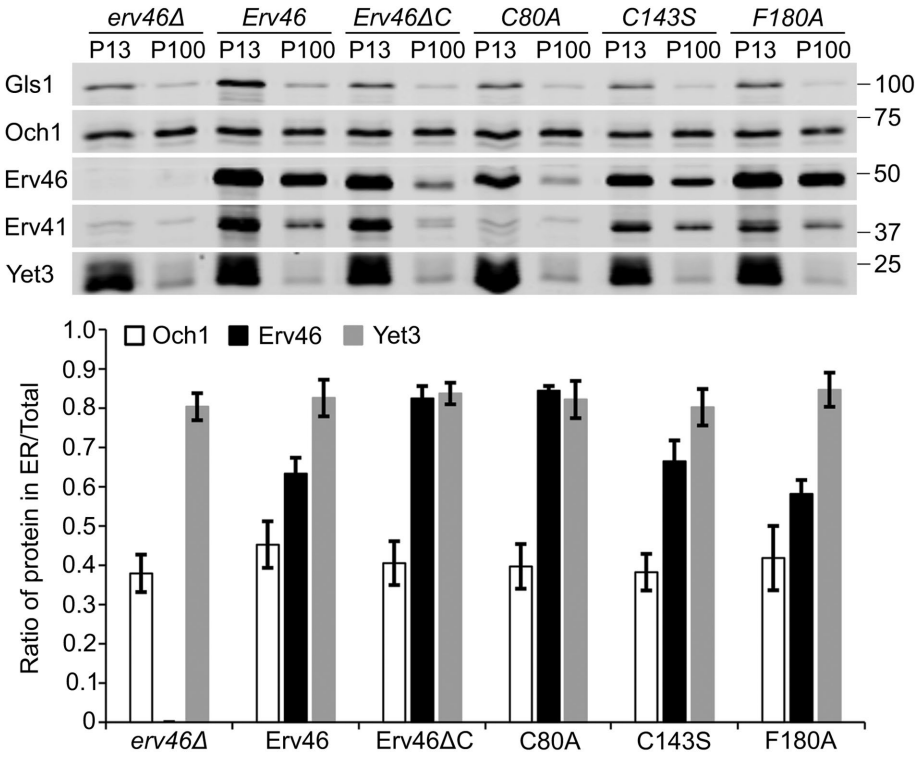

FIGURE 4: Subcellular distribution of wild-type and mutant Erv46 proteins. Cell lysates of an *erv46Δ* strain (CBY799) expressing wild-type or indicated Erv46 mutants from pRS316 plasmids were prepared and processed as described in *Materials and Methods*. The P13 (13,000 × *g*) and P100 (100,000 × *g*) pellets, which represent ER and Golgi-enriched fractions respectively, were resolved by SDS–PAGE and immunoblotted for indicated proteins. The ER marker Yet3 and Golgi marker Och1 show enrichment efficiency. Erv46ΔC was used as a control for ER trapped Erv46. Bar graph plots the ratio of each protein in the ER showing mean ($n = 3$) and standard error. Note that mutation of the ER export signal (Erv46ΔC) or the structural disulfide (C80A) shifted Erv46 to ER fractions, whereas other mutants were distributed between ER and Golgi membranes.

Escherichia coli using the pQE30 6His expression system (Supplemental Figure S5). Previous binding assays had used immobilized GST-Gls1 to monitor pH-dependent binding of the Erv41-Erv46 complex (Shibuya *et al.*, 2015), although production of purified GST-Gls1 was a limiting resource. Use of immobilized Fpr2 as the cargo ligand facilitates this assay. To ensure that binding between the Erv41-Erv46 complex and the immobilized Fpr2 was biologically relevant, we first tested the effect of pH on binding (Figure 7). 3HA-Erv46 from detergent-solubilized microsomes was efficiently recovered on Fpr2-agarose beads at pH 5.5 and 6.5; however, at pH 7.5, only background levels of 3HA-Erv46 were detected. To monitor background binding, we prepared agarose beads that had been reacted with Tris as the primary amine and then equilibrated the beads in binding buffer at pH 6.5. Minimal binding of 3HA-Erv46 to the Tris-agarose beads at pH 6.5 was observed, supporting dependence on immobilized Fpr2 for efficient binding (Figure 7). Moreover, abundant ER membrane proteins, including Yet3 and Gls2, were not recovered on the Fpr2-agarose beads at either pH, demonstrating specificity of the Fpr2-bead binding assay.

We next conducted experiments to monitor binding of Erv46 point mutants to immobilized Fpr2 in comparisons to wild-type Erv46 protein. The subsequent binding assays were performed at pH 6.5, which is thought to more closely reflect Golgi pH (Paroutis *et al.*, 2004). As expected, the C80A and C206A mutants that disrupt a predicted structural disulfide bond in Erv46 and produce misfolded proteins were inefficiently recovered on Fpr2-agarose beads compared with wild-type Erv46 (Figure 8A). In contrast, the C143S and C163S mutants that disrupt the first and second vicinal cysteine pairs in Erv46 bound as efficiently as wild-type Erv46 to the Fpr2-agarose beads (Figure 8B).

In vitro binding assay demonstrates that cargo binding depends on Erv46 hydrophobic residues

To directly measure cargo binding to wild-type Erv46 and mutant versions of Erv46, we developed an in vitro assay using the purified Fpr2 cargo protein immobilized on NHS-activated agarose beads. Fpr2 was expressed and milligram quantities were purified from

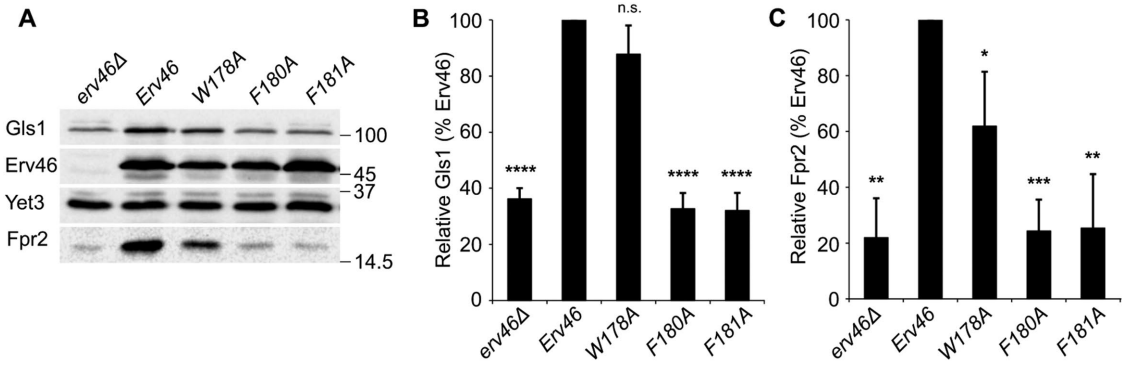

FIGURE 5: Erv46 hydrophobic mutants decrease retrieval activity. (A) Immunoblot and (B) quantification of Gls1 ($n = 3$) and (C) Fpr2 ($n = 3$) levels from whole cell extracts. Erv46 and mutant proteins were expressed from pRS316 plasmids in an *erv46Δ* background (CBY799). Gls1 and Fpr2 were normalized to the Yet3 loading control and plotted as a percentage relative to wild type. Error bars represent SEM and one-way ANOVA used to compare each mutant to wild type with *p* values of ****$p < 0.0001$, ***$p < 0.001$, **$p < 0.01$, *$p < 0.05$; n.s., not significant.

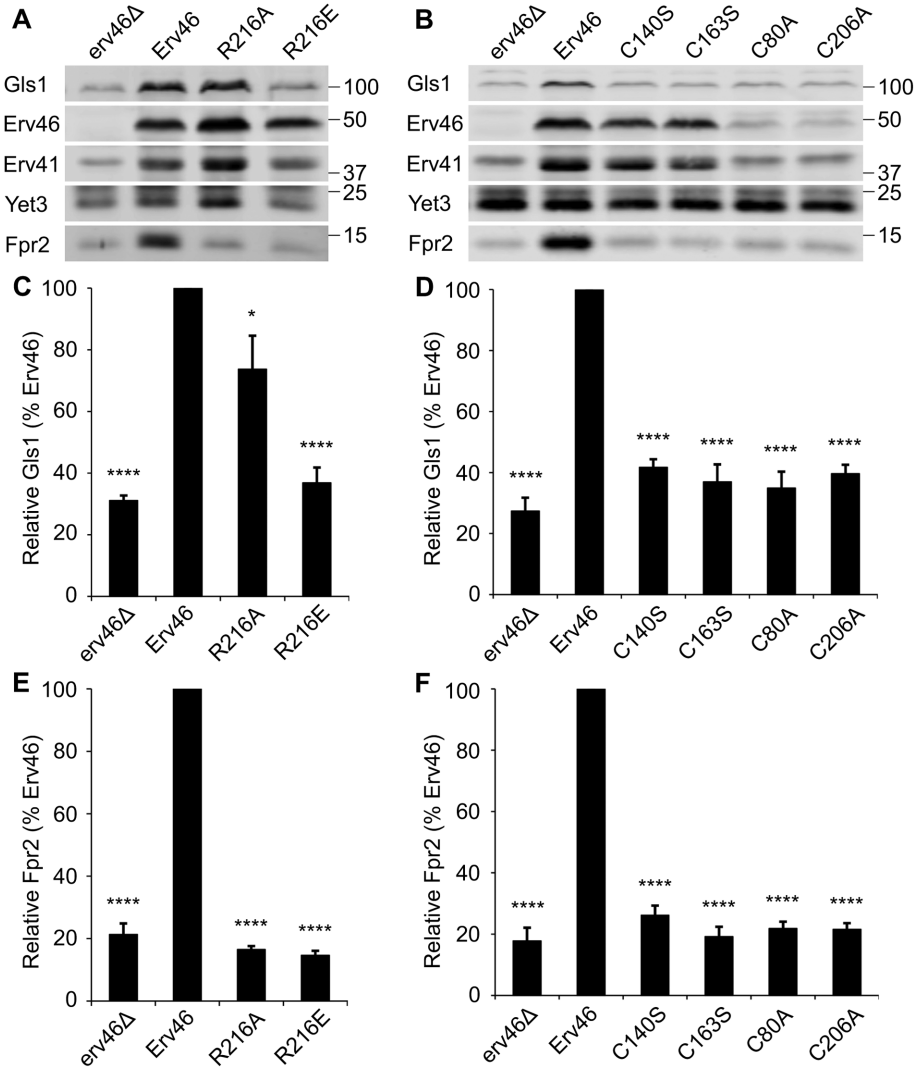

FIGURE 6: Retrieval activity of Erv46 R216 mutants and structural cysteine mutants. Immunoblot (A, B) and quantification (C–F) of Gls1 and Fpr2 steady state levels from whole cell extracts. Erv46 and indicated mutants were expressed from pRS316 plasmids in an *erv46Δ* background (CBY799). Gls1 and Fpr2 were normalized to the loading control Yet3 and plotted as a percentage of wild type. For C and E ($n = 3$) and D and F ($n = 4$), error bars represent SEM. One-way ANOVA was used to compare each mutant to wild type with ****$p < 0.0001$ and *$p < 0.05$.

Moreover, binding was specific as similar background binding to Tris-agarose beads was detected for the wild-type and cysteine mutant proteins. This was a surprising result and suggested that the vicinal cysteine pairs are not strictly required for binding to specific cargo, although their activity could regulate Erv46 conformation or access to Erv46-binding residues.

To further examine the binding properties of Erv46 cysteine mutants in cells, we measured the amount of bound Gls1 cargo using a coimmunoprecipitation (co-IP) assay from detergent-solubilized cell extracts (Shibuya *et al.*, 2015). As observed in Figure 8C, IP of HA-tagged Erv46 wild-type protein and C140S mutant yielded equivalent amounts of target protein. However, the level of Gls1 bound to the C140S mutant was significantly higher than the wild-type protein. This striking result suggests that the cysteine mutants can bind cargo efficiently in cells and may form tighter complexes or may be deficient in cargo release during passage through the ER.

We also tested binding of the Erv46 hydrophobic mutants (W178A, F180A, and F181A) to Fpr2 beads. While each of the three single-point mutants was recovered at similar levels as wild-type 3HA-Erv46, conversion of all three residues to alanines (WAFF>AAAA) resulted in a form of 3HA-Erv46 that was not efficiently bound by Fpr2 beads (Figure 9A). This finding suggests that the single mutations did not decrease binding affinity below the concentration of Fpr2 present in the in vitro binding assay but that converting the full stretch of hydrophobic residues in the triple mutant abolished binding. The results further suggest the hydrophobic patch is located on a surface-exposed region of Erv46 that interacts with cargo.

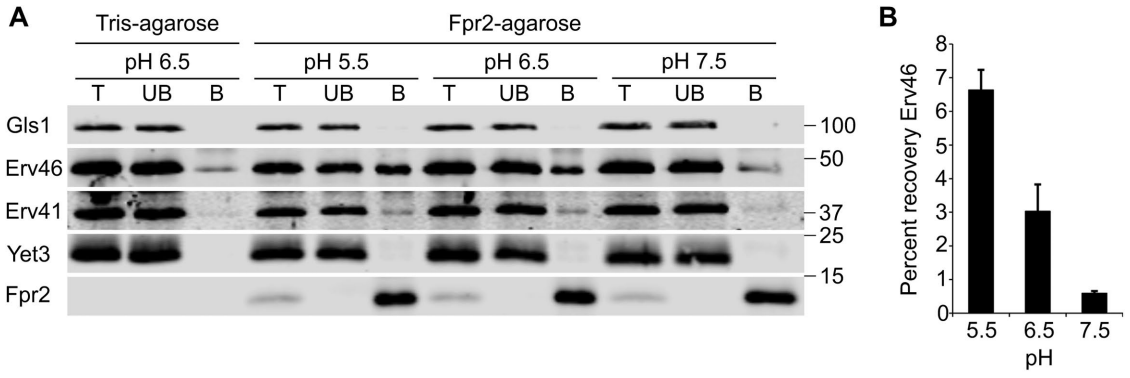

FIGURE 7: pH-dependent binding of Erv46 to immobilized Fpr2. Purified Fpr2 coupled to agarose beads was incubated with detergent-solubilized microsomes from strain CBY795 overexpressing Erv41 and Erv46 from pRS425-Erv41 and pRS426-Erv46. Binding reactions were carried out at the indicated pH and beads were washed at the same pH. Lanes represent (T) total binding reactions, (UB) unbound fractions after a brief spin to pellet Fpr2-agarose beads, and (B) bound fractions after washing. Tris-agarose served as a negative control. The bar graph plots the percentage of recovery of Erv46 relative to total at each pH and shows the mean ($n = 3$) and standard error.

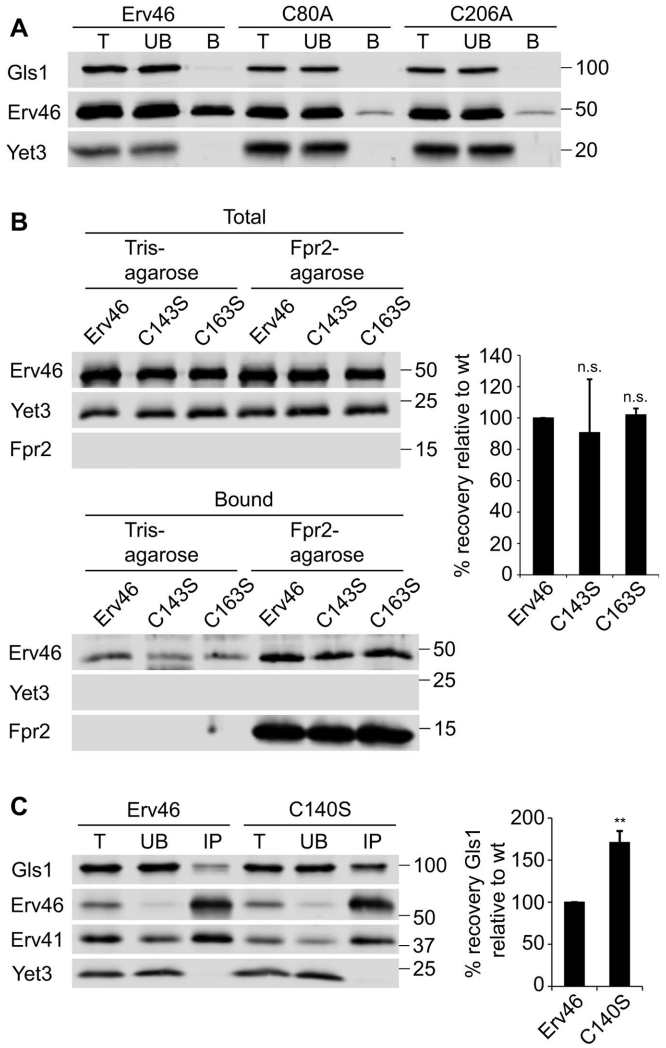

FIGURE 8: Erv46 cysteine mutants bind cargo in vitro and in vivo. Fpr2-agarose binding assays were conducted at pH 6.5 as described in Figure 7. Microsomes from cells overexpressing Erv41 (pRS425-Erv41) and wild-type or cysteine mutants of Erv46 (in pRS426-Erv46) were solubilized with detergent and extracts were incubated with Fpr2-agarose beads. (A) Structural cysteine mutants C80A and C206A in Erv46 failed to bind Fpr2. (B) The C143S and C163S mutants bind to Fpr2-agarose and quantification ($n = 3$) showed that mutant binding was similar to wild type. Binding was quantified by measuring bound Erv46 over total Erv46 and plotted as a percentage relative to wild type. Error bars represent SEM and one-way ANOVA comparing each mutant to wild type indicated p values that were not significantly different. Tris-agarose serves as a background control. (C) Native co-IP of HA-tagged Erv46 and C140S mutant. Semi-intact cells (CBY795) expressing Erv41 (pRS424-Erv41) and Gls1 (pRS426-Gls1) plus HA-tagged Erv46 (pRS425-pTPI-3HA-Erv46) or cysteine mutant (pRS425-pTPI-3HA-Erv46-C140S) were solubilized with detergent and immunoprecipitated with anti-HA antibody. Lanes represent (T) total, (UB) unbound material after centrifugation and immunoprecipitated (IP) material after washing antibody complexes bound to Protein A Sepharose beads. The plot shows the percentage of recovery of Gls1 relative to wild-type Erv46 with error bars representing SEM ($n = 4$) and one-way ANOVA used to compare the mutant to wild type (**$p < 0.01$). Note increased level of Gls1 coimmunoprecipitated with the C140S mutant.

Erv46 is necessary and sufficient to bind cargo in vitro

We had observed that Erv41 was recovered less efficiently than Erv46 in cargo binding assays using GST-Gls1 (Shibuya *et al.*, 2015) and Fpr2 (Figure 7). We speculated that the Erv46 subunit binds directly to cargo and when Erv41-Erv46 complexes are bound to Fpr2 agarose beads, much of the Erv41 subunit dissociates when the beads are washed. To test this possibility, we conducted the Fpr2-agarose binding assays using detergent-solubilized microsome extracts prepared from *erv41*Δ strains. Owing to the lowered expression levels of Erv46 in the absence of Erv41, we used strains overexpressing Erv46 or the Erv46 WAFF>AAAA mutant as a negative control. In extracts from *erv41*Δ cells, Erv46 was efficiently bound by Fpr2-agarose to the same extent as in the wild-type background (Figure 9B). As expected, the WAFF>AAAA mutant was not efficiently recovered on Fpr2-beads when expressed in the *erv41*Δ background. These combined results further support the model that Erv46 is sufficient for cargo binding, whereas Erv41 may regulate but is not required for cargo binding interactions.

Stoichiometry of the Erv41-Erv46 complex

Quantitative mass spectrometry-based proteomic approaches report that budding yeast contain 2096 molecules of Erv41 and 3863 molecules of Erv46 per cell (Kulak *et al.*, 2014). Similarly, HeLa cells have 71,806 copies of Erv41/ERGIC2 and 160,266 copies of Erv46/ERGIC3 (Kulak *et al.*, 2014). The approximate 1:2 ratio of Erv41 to Erv46 in both species suggests that the Erv41-Erv46 complex contains two copies of Erv46 for each copy of Erv41. Furthermore, sedimentation on sucrose gradients shows that the Erv41-Erv46 complex migrates slightly larger than the 100 kDa maker (Welsh *et al.*, 2006). Taken together, these data suggest that the Erv41-Erv46 complex is a trimer consisting of a single copy of Erv41 and two copies of Erv46. To test this model, we conducted co-IP experiments from wild-type yeast cells containing plasmids that expressed either HA-Erv41 or HA-Erv46. The trimer model predicts that HA-Erv46 should assemble into complexes with endogenous untagged Erv46, whereas the HA-Erv41 should assemble into complexes with Erv46 but not with endogenous untagged Erv41. As shown in Figure 10, IP of HA-Erv46 recovered both endogenous Erv41 and Erv46. In contrast, IP of HA-Erv41 coprecipitated endogenous Erv46 but no endogenous Erv41 was detected. These findings support the model that Erv41-Erv46 complex consists of a single copy of Erv41 and two copies of Erv46.

DISCUSSION

Here we exploited molecular genetic and biochemical approaches to dissect function of the conserved cysteine-rich region in Erv46/ERGIC3. This protein family contains an unusual thioredoxin-like domain with conserved CXXC and CCXXC motifs. Whereas HHPred aligns this first CXXC motif with PDI proteins, Erv46 lacks typical **a**, **b**, **b'** or **a'** thioredoxin-like domains found in PDI family members (Hatahet and Ruddock, 2009). Interestingly, plants have additional Erv46 isoforms (PDI-C subfamily) in which the cysteine-rich region contains the canonical **a**-type thioredoxin-like domain (Yuen *et al.*, 2016). These sequence homologies suggest potential redox regulation of Erv46 family members. To investigate Erv46 retrieval mechanisms, we introduced point mutations into the six conserved cysteine residues for in vivo and in vitro analysis. Each of the cysteine residues in this domain is required for cellular function as the point mutations produced defects in ER retention of Gls1 and Fpr2 that were equivalent to an *erv46*Δ strain. The cysteine to serine mutations produced stable forms of Erv46 that assembled into complexes with

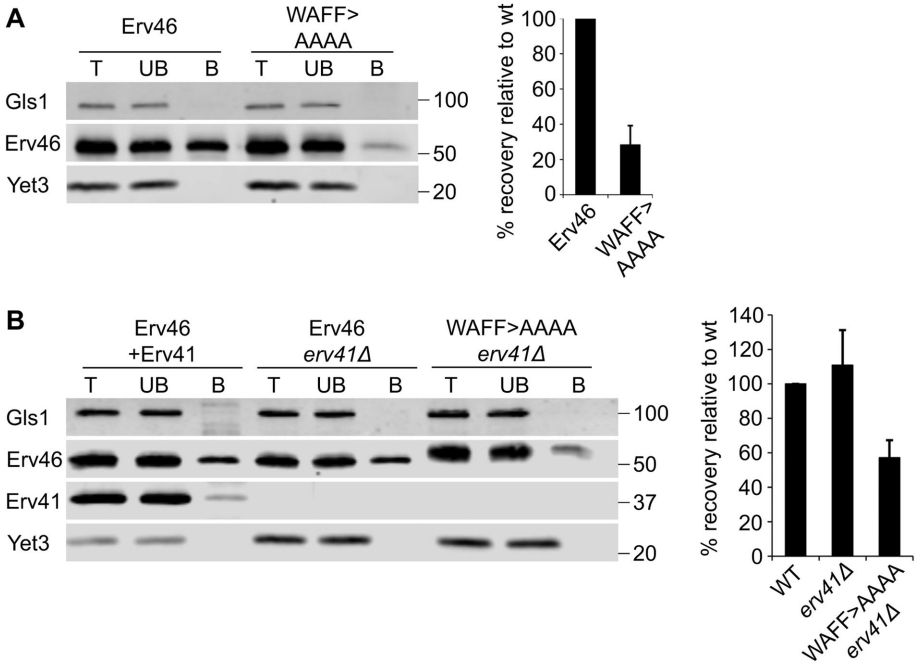

FIGURE 9: Erv46 hydrophobic mutants fail to bind Fpr2 in vitro. Fpr2-agarose binding assays using Erv46 from detergent-solubilized microsomes at pH 6.5. (A) Cells (CBY795) overexpressing Erv41 (pRS424-Erv41) and HA-tagged versions of wild-type (pRS425-pTPI-3HA-Erv46) or the hydrophobic Erv46 mutant (pRS425-pTPI-3HA-Erv46-AAAA) were used. The bar graph shows the percentage of recovery of Erv46 protein relative to wild type with standard error ($n = 3$). Note the WAFF>AAAA mutation diminished binding to Fpr2-agarose. (B) Fpr2-agarose binding assays using extracts from cells overexpressing Erv41 (pRS424-Erv41) and HA-tagged Erv46 (pRS425-pTPI-3HA-Erv46) compared with cells that do not express Erv41 in the *erv41Δ* background (CBY797) but do express HA-tagged Erv46 (pRS425-pTPI-3HA-Erv46) or the hydrophobic mutant WAFF>AAAA. Bar graph plots the percentage of recovery relative to wild-type Erv46 and shows standard error ($n = 3$). Note that Erv46 binds Fpr2-agarose in the absence of Erv41.

the Erv41 subunit and cycle between ER and Golgi compartments. However, the cysteine to serine point mutations in Erv46 produced striking changes when resolved on nonreducing PAGE revealing more reduced monomeric forms compared with wild-type protein in addition to higher molecular weight mixed-disulfide species. These mixed-disulfide forms could be Erv46 multimers as observed for thioredoxin-active site mutants (Kouwen *et al.*, 2008) or cross-linked adducts between Erv46 and other ER luminal proteins. Erv46 specific cargo (e.g., Gls1 or Fpr2) was not detected in the higher molecular weight mixed mixed-disulfide forms. On the basis of these findings, we propose that redox status of the cysteine-rich region of Erv46 regulates cargo binding.

PEG-Mal treatment of wild-type Erv46 in cell lysates indicates that the six conserved cysteine residues are largely in disulfide linkages under steady-state conditions. However, when single cysteine to serine mutations are introduced, PEG-Mal treatment produced highly modified and heterogenous forms of Erv46 indicating the presence of multiple free sulfhydryl groups. We speculate that removal of a single disulfide linkage in the cysteine-rich region disrupts normal disulfide pairing and causes Erv46 to cycle through various redox states. Because the cysteine mutants are not apparently retained in the ER and are not directed to ER-associated degradation (Mehrtash and Hochstrasser, 2018), these reduced forms could represent intermediates in the Erv46 cargo retrieval cycle.

In contrast to the cysteine mutants, conserved hydrophobic residues (W178, F180, and F181) within this cysteine-rich region are required for Erv46 function but did not alter the redox status of Erv46 on nonreducing gels. To directly test cargo binding properties of these different types of Erv46 mutants, we immobilized the Fpr2 ligand on agarose beads and measured pH-dependent binding of wild-type and mutant Erv46 proteins. In vitro binding assays showed that the hydrophobic residues were required for binding to Fpr2 although surprisingly the cysteine mutants (C143S and C163S) remained active for cargo interaction. Moreover, we have observed that the addition of 5 mM dithiothreitol (DTT) to in vitro binding reactions with wild-type Erv46 did not decrease cargo binding, suggesting that reduction of disulfide linkages within the cysteine-rich region of Erv46 does not inhibit cargo binding. Finally, we find increased levels of bound Gls1 cargo in complex with the Erv46 C140S mutant when isolated from cell extracts. One possible explanation for these findings is that specific disulfide-linked arrangements alter the conformational state of Erv46 in a manner that regulates cargo binding. Redox status is well known to regulate ER–protein activity (Ellgaard *et al.*, 2018). For Erv46, a distinct pairing of disulfide bonds could expose hydrophobic residues for cargo binding at the reduced pH of Golgi compartments. After retrograde transport of Erv46-cargo complexes, the presence of oxidoreductases in the ER (e.g., Pdi1 and family members) could transiently reconfigure

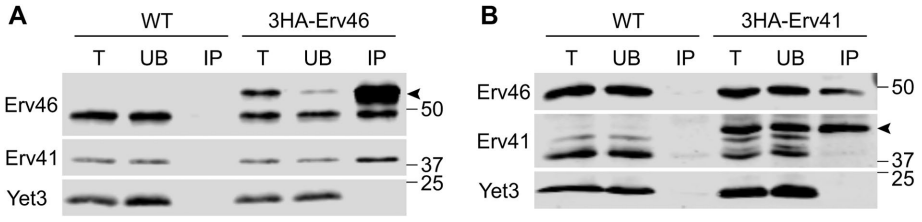

FIGURE 10: Co-IP of HA-tagged Erv46 and HA-tagged Erv41 expressed from plasmids in wild-type cells. (A) Semi-intact cells (CBY740) expressing empty vector (pRS425) or HA-tagged Erv46 (pRS425-3HA-Erv46) were solubilized with digitonin and co-IPs conducted with anti-HA antibody. Lanes represent (T) total reactions, (UB) unbound material after centrifugation, and (IP) immunoprecipitated material after washing antibody complexes bound to Protein A Sepharose beads. Note that HA-Erv46 coimmunoprecipitated endogenous Erv46 and Erv41. (B) Semi-intact cells from an untagged diploid strain (CBY763) or expressing HA-tagged Erv41 (CBY782) were solubilized with digitonin and IPs conducted with anti-HA antibody as in panel A. Note, HA-Erv41 coimmunoprecipitated endogenous Erv46 but not endogenous Erv41. Arrows indicate HA-tagged Erv46 and HA-tagged Erv41 for A and B, respectively. Yet3 serves as a specificity control for the IPs.

disulfide linkages and trigger the release of bound cargo in the ER. If proper disulfide bonds are not present, as in the cysteine mutants, cargo release may be inefficient and the occupied Erv46 receptor would not function in its normal retrieval cycle. This model and alternative models await further testing in refined assays.

The Erv46 cargo binding cycle bears some resemblance to ERp44, which is a retrograde receptor for escaped ER residents and incompletely folded secretory cargo (Anelli *et al.*, 2015). However, ERp44 is a clear PDI family member containing thioredoxin-like **a**, **b**, and **b'** domains with C29 in the **a** domain active in formation of mixed-disulfide linkages with its clients (Anelli *et al.*, 2003; Wang *et al.*, 2008). ERp44 is also a soluble luminal protein and the lower pH of *cis*-Golgi compartments induces a conformational change that exposes the cargo binding site as well as its C-terminal RDEL retrieval motif (Vavassori *et al.*, 2013). In this manner, pH controls binding of escaped ER proteins to ERp44 and linkage to the KDEL receptor for retrograde transport to the ER in COPI vesicles. More recent reports reveal that ERp44 employs a redox-dependent binding and release mechanism to recycle cargo (Yang *et al.*, 2016). Although ERp44 and Erv46 may use analogous pH and redox gradients to control their cargo binding cycle, the molecular features and underlying mechanism are clearly distinct.

Luminal pH plays prominent roles in regulating cargo binding to retrograde receptors in the secretory pathway. Studies have shown that histidine residues, which can undergo ionization in the pH 6–7 range, are important for pH-dependent control of cargo binding in many receptors including the LDL receptor (Huang *et al.*, 2010), KDEL receptor (Brauer *et al.*, 2019), and ERp44 (Watanabe *et al.*, 2017). In some instances, single conserved histidine residues are critical, whereas in other cases, clusters of histidine residues are involved (Huang *et al.*, 2010; Watanabe *et al.*, 2017). Erv46 contains several highly conserved histidine residues; however, mutation of these individual residues did not produce a detectable loss in retrieval activity. It may be that multiple histidine mutations are required to impact Erv46 cellular function or that other pH-sensitive residues (e.g., cysteine, glutamate) contribute to pH-dependent binding activity. Regardless, the membrane topology and unique domains of the Erv41-Erv46 complex suggest a novel binding cycle compared with other retrograde receptors.

Our results indicate that Erv46 is sufficient for cargo binding in vitro although the native Erv41-Erv46 complex likely contains two copies of Erv46 and a single copy of Erv41. A recent study of ERGIC3, the human orthologue of Erv46, supports a similar subunit arrangement with ERGIC2/Erv41 (Yoo *et al.*, 2019). However, the role for Erv41 in this cargo retrieval cycle remains to be determined. Erv41 could be involved in negatively regulating access to the Erv46 hydrophobic binding site when cycling through the ER. Alternatively, Erv41 could serve a primary role in bidirectional trafficking of the Erv41-Erv46 complex. Both C-terminal cytoplasmic tail sequences of Erv41 and Erv46 are functionally required in a specific orientation for efficient export of the complex from the ER as well as retrieval back to the ER from the Golgi (Otte and Barlowe, 2002). Therefore, Erv41 could function in regulating transport of the complex, depending on occupancy of its cargo binding site. For example the KDEL-receptor is redistributed from Golgi to ER membranes when KDEL ligands are elevated (Lewis and Pelham, 1992), and structural studies show that binding of the KDEL peptide rearranges the receptor to expose a potent dilysine motif for COPI-dependent retrieval (Brauer *et al.*, 2019). Cargo binding to Erv41-Erv46 in Golgi compartments could similarly reconfigure the complex to make the Erv46 dilysine signal available for COPI recognition. Structural and biochemical approaches will be needed to fully define underlying mechanisms and progress in isolating purified forms of the Erv46 luminal domain and Erv41-Erv46 complex should advance these goals.

MATERIALS AND METHODS

Yeast strains and growth media

Yeast strains used in this study are listed in Table 1 and were transformed with plasmids (listed in Supplemental Table S1) using a standard lithium acetate transformation protocol (Elble, 1992). Yeast precultures were grown overnight at 30°C in selective media containing 0.7% yeast nitrogen base without amino acids, 2% glucose, and appropriate supplement mixture (MP Biomedicals). Precultures were back diluted into fresh YPD (1% Bacto yeast extract, 2% Bactopeptone, and 2% glucose) at an absorbance of 0.1 at 600 nm (OD_{600}). Cells were cultured at 30°C either by rotation of culture tubes on a wheel or in flasks in a shaker incubator for larger cultures. Absorbance was monitored until cells reached an OD_{600} between 0.8 and 1.2.

Antibodies

For primary antibodies, rabbit polyclonal antiserum against Erv41, Erv46, and Och1 (Otte *et al.*, 2001); Yet3 (Wilson and Barlowe, 2010); Fpr2; and Gls1 (Shibuya *et al.*, 2015) has been described previously. Mouse monoclonal antibody HA.11 against the hemagglutinin epitope was purchased from BioLegend (San Diego, CA) and used for co-IPs and detection of HA-tagged proteins by immunoblot. Primary antibodies were used at 1:1000 dilutions except for anti-Fpr2 and anti-HA, which were used at 1:500 and 1:2000 dilutions, respectively. For secondary antibodies, two different systems were used. First, horseradish peroxidase–linked anti-rabbit and

Strain	Genotype	Reference
FY833	*MATa his3Δ200 ura3-52 leu2Δ1 lys2Δ202 trp1Δ63*	Winston *et al.*, 1995
FY834	*MATα his3Δ200 ura3-52 leu2Δ1 lys2Δ202 trp1Δ63*	Winston *et al.*, 1995
CBY453	FY833 × FY834	Powers and Barlowe, 1998
CBY740 (BY4742)	MATα his3Δ1 leu2Δ0 lys2Δ0 ura3Δ0	Winzeler *et al.*, 1999
CBY763	CBY453 diploid with ERV41/erv41Δ::HIS3	Otte *et al.*, 2001
CBY782	CBY453 diploid with ERV41/ERV41Δ::TRP-PGAL1-3HA	Otte *et al.*, 2001
CBY795	FY834 with erv41Δ::HIS3 erv46Δ::kanR	Otte *et al.*, 2001
CBY797	FY834 with erv41Δ::HIS3	Otte *et al.*, 2001
CBY799	FY834 with erv46Δ::kanR	Otte *et al.*, 2001

TABLE 1: Yeast strains used in the study.

anti-mouse antibodies (GE Healthcare) were used at 1:10,000 dilutions. Blots were developed with SuperSignal West Pico Chemiluminescent substrate (Thermo Fisher Scientific), imaged using a G:Box Chemi XR5 (Syngene), and quantified with GeneTools image analysis software (Syngene). Alternatively, IRDye cross-linked anti-rabbit and anti-mouse antibodies (LI-COR Biosciences) were used at 1:10,000 dilutions. Blots were imaged with an Odyssey CLx imager (LI-COR Biosciences) and quantified with Image Studio Lite (LI-COR Biosciences).

Semi-intact cell and microsome preparations

Yeast semi-intact cells were prepared using methods similar to those previously described (Baker *et al*., 1988). Briefly, cells were grown to approximately 1.0 OD_{600} and harvested by centrifugation (3500 rpm, 4 min, SS-34 rotor) at room temperature. Cell pellets were resuspended in buffer (100 mM Tris, pH 9.4, 5 mM DTT) for 10 min at room temperature. Cells were pelleted as before and cell pellets were resuspended in lyticase buffer (20 mM Tris, pH 7.5, 0.7 M sorbitol, 0.5% glucose, 2 mM DTT) before the addition of lyticase. After the addition of lyticase, spheroplast conversion was monitored by change in OD_{600} until 90% complete (approximately 10 min) and then spheroplasted cells were diluted into ice-cold lyticase buffer followed by centrifugation at 5000 rpm in an SS-34 rotor for 5 min at 4°C. Spheroplasts were resuspend in lysis buffer (20 mM HEPES, pH 7.0, 0.1 M sorbitol, 150 mM KOAc, 2 mM $Mg(OAc)_2$), aliquoted, frozen in liquid N_2, and stored at –80°C. Yeast ER microsomes were prepared using methods described previously (Wuestehube and Schekman, 1992). Briefly, spheroplasts were prepared as above but were resuspended in JR lysis buffer (20 mM HEPES, pH 7.4, 0.1 M sorbitol, 50 mM KOAc, 2 mM EDTA, 1 mM DTT, 1 mM paramethylsulfonyl fluoride [PMSF]) and lysed with a Dounce homogenizer. To remove unbroken cells, lysates were centrifuged at 3500 rpm at 4°C for 5 min in an SS-34 rotor. The supernatant was transferred to a fresh tube and centrifuged as before but at 15,000 rpm for 10 min. The membrane pellet was resuspended in minimal JR lysis buffer and layered on top of a two-step sucrose gradient (1.2/1.5 M sucrose in 20 mM HEPES, pH 7.4, 50 mM KOAc, 2 mM EDTA) and centrifuged at 40,000 rpm for 1 h at 4°C in an SW-60 rotor (Beckman Coulter). ER microsomes sedimented between the 1.2 and 1.5 M sucrose interface. The ER microsome band was collected and diluted in B88 (20 mM HEPES, pH 6.8, 250 mM sorbitol, 150 mM KOAc, 5 mM $Mg(OAC)_2$). ER microsomes were pelleted at 15,000 rpm at 4°C for 10 min in an SS-34 rotor and membrane pellets were resuspended in B88 before snap freezing in liquid N_2 and storage at –80°C.

Plasmid construction

Plasmids generated in this study are listed in Supplemental Table S1. To construct Erv46 mutant plasmids, the "megaprimer" site-directed mutagenesis method was used (Sarkar and Sommer, 1990). Briefly, each mutagenesis reaction required three primers: a forward primer upstream of the start codon, a reverse primer downstream of the stop codon, and a mutagenic primer in either the forward or the reverse direction. The forward and reverse primers were designed to anneal 300 base pairs upstream or downstream from the start and stop sites, respectively, and were engineered to contain *Sac*I and *Xba*I restriction sites, respectively. A first round of PCR was carried out with the mutagenic primer and the appropriate upstream or downstream primer. The pRS316-Erv46 plasmid (Otte *et al*., 2001) was used as the template for single mutants. After gel purification (Omega Bio-tek, Norcross, GA), a second PCR was carried out with the "megaprimer" product from the first PCR and the remaining primer. The final product was gel purified, digested with *Sac*I and *Xba*I, heated to inactivate the restriction enzymes, and ligated into pRS316 linearized with the same restriction enzymes. Multiple cysteine mutants were constructed by replacing the template pRS316-Erv46 with an iteration of the same plasmid but containing cysteine mutations. The hydrophobic patch triple mutant was made using a mutagenic primer containing all three mutations. To generate pRS425-pTPI-3HA-Erv46, the Erv46 open reading frame with adjacent *Bam*HI and *Sal*I sites was inserted into pRS426. A synthetic gene fragment (IDT, Coralville, IA) containing the 3xHA tag flanked by *Bam*HI sites was inserted into the start site of Erv46. 3HA-Erv46 was then transferred into the *Xma*I-*Sal*I site of pRS425-pTPI (Anderson and Barlowe, 2019). For the 6His-tagged Fpr2 expression construct, Fpr2 was cloned from pGEX2T-Fpr2 (Shibuya *et al*., 2015) into pQE30 to produce pQE30-Fpr2. The Fpr2 endogenous stop codon (TAG) was replaced by three stop codons (TAATAATGA) to prevent read-through. This insertion was included in the reverse primer. All constructs were verified by DNA sequencing.

Mutant analysis by reducing and nonreducing SDS–PAGE

For whole-cell lysates, 1.0 OD_{600} of cells was pelleted. Cell pellets were resuspended in 75 µl of 20 mM NaN_3, 1 mM PMSF, and an equal volume of SDS–PAGE sample buffer (125 mM Tris, pH 6.8, 25% glycerol, 4% SDS, 5% β-mercaptoethanol, bromophenol blue), and 0.5-mm glass beads were added. Cells were lysed in a Mini-Beadbeater (Biospec, Bartlesville, OK) for 2 min at 4°C, followed by heating to 95°C. Cell lysates were resolved by SDS–PAGE and transferred to nitrocellulose membranes for immunoblotting. To preserve disulfide species, semi-intact cells were washed into cold Tris-buffered saline (TBS) with NEM (50 mM Tris, pH 7.5, 150 mM NaCl, 10 mM NEM) at 4°C followed by resuspension into TBS with NEM and solubilized with equal parts SDS–PAGE sample buffer lacking β-mercaptoethanol. Solubilized extracts were resolved by SDS–PAGE on 7.5% acrylamide gels and transferred to nitrocellulose membranes for immunoblotting.

Protein PEGylation

Yeast semi-intact cells were pegylated with methoxypolyethylene glycol maleimide 5000 (PEG-Mal5k; Sigma-Aldrich) as follows. Semi-intact cells (1.0 OD_{280}) were centrifuged at 14,000 rpm for 5 min at 4°C in an Eppendorf 5424 centrifuge. Semi-intact cell pellets were then washed by resuspension on ice with 250 µl of cold TBS + PEG-Mal5k (50 mM Tris, pH 7.5, 150 mM NaCl, 4 mM PEG-Mal 5k). Suspensions were left on ice for 5 min before centrifugation as before. Cell pellets were then resuspended in 15 µl of the same PEG-Mal5k containing TBS buffer but with the addition of 1% SDS on ice, vortexed, and then heated to 37°C for 20 min. SDS–PAGE sample buffer (5 µl) was added to the sample, which was then boiled for 5 min. PEGylated samples were resolved on standard SDS–PAGE reducing gels and transferred to nitrocellulose membranes for immunoblotting. Blotting against Och1, a Golgi-localized protein containing a single cysteine, was used to monitor efficiency of the PEGylation reaction.

P13/P100 fractionation

ER- and Golgi-enriched fractions were prepared in a similar manner outlined previously (Belden and Barlowe, 2001). Yeast strains were grown overnight in selective media followed by back dilution into 25 ml of YPD the following morning. Cells were grown to OD_{600} = 1.0 and harvested as described under semi-intact cell preparation. After converting to spheroplasts, cells were resuspended in JR lysis buffer (20 mM HEPES, pH 7.4, 0.1 M sorbitol, 50 mM KOAc, 2 mM EDTA, 1 mM DTT, 1 mM PMSF) and lysed with a Dounce homogenizer.

Samples were centrifuged at 2000 rpm for 5 min at 4°C in an SS-34 rotor to remove unbroken cells. The resulting supernatant was centrifuged at 14,000 rpm for 10 min at 4°C in an Eppendorf 5424 centrifuge to obtain the ER-enriched P13 pellet fraction. The supernatant fraction was transferred to a fresh tube and centrifuged at 60,000 rpm for 15 min at 4°C in a Beckman TLA 100.3 rotor to obtain the Golgi-enriched P100 pellet fraction. Both pellet fractions were resuspended in 100 µl of 20 mM Tris, pH 7.5, 20 mM NEM and then 100 µl of SDS–PAGE sample buffer was added. ER- and Golgi-enriched fractions were resolved by SDS–PAGE and immunoblotted. The ER marker Yet3 and the Golgi marker Och1 were used to monitor fractionation efficiency, whereas the ER export-deficient Erv46ΔC served as a negative control (Otte and Barlowe, 2002).

Fpr2 purification/Fpr2-agarose/Fpr2-agarose binding assay

Fpr2 used in Fpr2-agarose binding assays was prepared using standard NiNTA affinity purification techniques. Briefly, 6His-tagged Fpr2 was expressed in *E. coli* by IPTG induction. XL1-Blue cells carrying pQE30-Fpr2 (CBB5564) were grown overnight in LB-Amp at 37°C. The overnight culture was used to inoculate 1.5 l of LB-Amp at 0.1 OD_{600}. Growth was monitored and when the culture reached an OD_{600} of 0.6, IPTG was added to a final concentration of 1 mM and grown for 3.5 h at 37°C. Cells were harvested by centrifugation and resuspended in ice-cold lysis buffer (50 mM Tris, pH 7.4, 150 mM NaCl, 20 mM imidazole). Cells were lysed using a French press and lysates were centrifuged in an SS-34 rotor at 14,000 rpm for 10 min at 4°C. The supernatant fraction was then centrifuged at 54,000 rpm for 30 min at 4°C in a 60 Ti fixed angle rotor (Beckman Coulter). The resulting high-speed supernatant was loaded on to a manually poured 5 ml NiNTA-agarose (Qiagen) column connected to an AKTA FPLC (GE-Life Sciences) that had been equilibrated in lysis buffer. Once bound to resin, the column was washed with 5 column volumes (CV) of lysis buffer followed by 8 CVs of lysis buffer with an increasing gradient of imidazole (20–400 mM). 6His-tagged Fpr2 eluted around 220 mM imidazole as monitored by A_{280} and further characterized by SDS–PAGE and Coomassie staining (Supplemental Figure S5).

Fpr2 was covalently linked to agarose (Fpr2-agarose) using NHS-activated agarose (Pierce) as follows. Purified 6His-tagged Fpr2 was dialyzed into cold phosphate-buffered saline (PBS; 50 mM sodium phosphate, pH 7.5, 150 mM NaCl). Dialyzed Fpr2 was recovered and centrifuged at 14,000 rpm for 5 min at 4°C to remove insoluble material. Protein was quantified by A_{280} using a NanoDrop Spectrophotometer (Thermo-Fisher Scientific) resulting in a concentration of approximately 1 mg/ml. Fpr2-agarose was prepared fresh by adding 0.1 ml of Fpr2/8 mg of dry NHS-agarose on ice. After 30 min, unbound material was quantified using Bio-Rad Bradford Reagent (Hercules, CA) and typically there was a >95% reduction in soluble Fpr2 resulting in about 40 µl of Fpr2-agarose resin containing 2–3 mg/ml Fpr2. The Fpr2-agarose beads were pelleted gently and blocked with 1 M Tris, pH 7.5, for 10 min on ice. Fpr2-agarose beads were then washed into an appropriate binding buffer. Tris-agarose was prepared by mixing NHS-agarose with 1 M Tris, pH 7.5, for 10 min on ice followed by equilibration into binding buffer.

To assay Erv46 binding to Fpr2-agarose, microsomes expressing Erv46 or Erv46 mutants were solubilized in binding buffer on ice for 10 min in PBST (50 mM sodium phosphate, 150 mM NaCl, 1% Triton X-100) at the indicated pH. Solubilized extracts were centrifuged at 14,000 rpm for 5 min, and the supernatant was applied directly to Fpr2-agarose or Tris-agarose equilibrated in the appropriate binding buffer. Binding reactions were incubated at 4°C with rotation for 30 min. A total fraction was collected and after gentle centrifugation at 4°C, the unbound material was removed. The Fpr2-agarose beads were then washed with ice-cold binding buffer 3×, and SDS–PAGE sample buffer was added to the resin. Binding activity was monitored by SDS–PAGE and immunoblotting of fractions. Total and unbound fractions loaded onto gels represent 10% of the bound material.

Co-IP of epitope-tagged Erv41 and Erv46

Native co-IP of proteins from diploid yeast strains with one untagged and one HA-tagged copy of Erv41 or from a wild-type haploid yeast strains with plasmid expressed HA-tagged Erv46 was conducted. Semi-intact cells were prepared and pelleted to remove B88. Semi-intact cell pellets were resuspended in IP buffer + 1% digitonin (20 mM HEPES, pH 8.0, 250 mM sorbitol, 150 mM KOAc, 5 mM $Mg(OAc)_2$, 1 mM PMSF, 1% digitonin wt/vol) and incubated at room temperature for 10 min with gentle mixing. Semi-intact cell lysates were centrifuged at 15,000 rpm for 5 min at 4°C in an Eppendorf 5424 centrifuge and the resulting supernatant was added to washed Protein A Sepharose beads (GE Life Sciences), followed by the addition of anti-HA.11 antibody. Co-IP was carried out for 1 h at 4°C with rotation. A total fraction was removed from this co-IP mixture and after gentle centrifugation an unbound fraction was also removed. The Protein A Sepharose beads were washed 3× with ice-cold IP buffer + 0.05% digitonin. Sample buffer was added to the beads and samples were resolved by SDS–PAGE and transferred to nitrocellulose membranes for immunoblotting. Total and unbound fractions represent 10% of the bead-bound IP material.

Native co-IP of HA-tagged Erv46 or C140S mutant to measure the level of bound Gls1 was carried out as follows. Semi-intact cells were prepared and pelleted to remove B88. Cells were then resuspended in TBST (50 mM Tris, pH 7.5, 150 mM NaCl, 1% Triton X-100) on ice for 10 min before centrifugation at 15,000 rpm for 5 min at 4°C in an Eppendorf 5424 centrifuge. The resulting supernatants were mixed with 0.5 µl of anti-HA.11 antibody and Protein A Sepharose beads for binding at 4°C for 1 h. A total fraction was removed from each sample before gentle centrifugation to prepare an unbound fraction for analysis by SDS–PAGE. The beads were washed 4× with ice-cold TBST before the addition of sample buffer followed by SDS–PAGE and transfer to nitrocellulose for immunoblotting. Total and unbound fractions represent 10% of the bead-bound IP material.

ACKNOWLEDGMENTS

This work was supported by National Institutes of Health Grant GM052549 and BioMT COBRE P20 GM1131132.

REFERENCES

Adolf F, Rhiel M, Hessling B, Gao Q, Hellwig A, Bethune J, Wieland FT (2019). Proteomic profiling of mammalian COPII and COPI vesicles. Cell Rep 26, 250–265.e255.

Anderson NS, Barlowe C (2019). Conserved juxtamembrane domains in the yeast golgin Coy1 drive assembly of a megadalton-sized complex and mediate binding to tethering and SNARE proteins. J Biol Chem 294, 9690–9705.

Anelli T, Alessio M, Bachi A, Bergamelli L, Bertoli G, Camerini S, Mezghrani A, Ruffato E, Simmen T, Sitia R (2003). Thiol-mediated protein retention in the endoplasmic reticulum: the role of ERp44. EMBO J 22, 5015–5022.

Anelli T, Sannino S, Sitia R (2015). Proteostasis and "redoxtasis" in the secretory pathway: Tales of tails from ERp44 and immunoglobulins. Free Radic Biol Med 83, 323–330.

Appenzeller-Herzog C, Roche AC, Nufer O, Hauri HP (2004). pH-induced conversion of the transport lectin ERGIC-53 triggers glycoprotein release. J Biol Chem 279, 12943–12950.

Baker D, Hicke L, Rexach M, Schleyer M, Schekman R (1988). Reconstitution of SEC gene product-dependent intercompartmental protein transport. Cell 54, 335–344.

Barlowe C, Helenius A (2016). Cargo capture and bulk flow in the early secretory pathway. Annu Rev Cell Dev Biol 32, 200–225.
Bartlett GJ, Porter CT, Borkakoti N, Thornton JM (2002). Analysis of catalytic residues in enzyme active sites. J Mol Biol 324, 105–121.
Belden WJ, Barlowe C (2001). Deletion of yeast p24 genes activates the unfolded protein response. Mol Biol Cell 12, 957–969.
Biterova EI, Svard M, Possner DD, Guy JE (2013). The crystal structure of the lumenal domain of Erv41p, a protein involved in transport between the endoplasmic reticulum and Golgi apparatus. J Mol Biol 425, 2208–2218.
Brauer P, Parker JL, Gerondopoulos A, Zimmermann I, Seeger MA, Barr FA, Newstead S (2019). Structural basis for pH-dependent retrieval of ER proteins from the Golgi by the KDEL receptor. Science 363, 1103–1107.
Elble R (1992). A simple and efficient procedure for transformation of yeasts. BioTechniques 13, 18–20.
Ellgaard L, Sevier CS, Bulleid NJ (2018). How are proteins reduced in the endoplasmic reticulum? Trends Biochem Sci 43, 32–43.
Gilbert HF (1990). Molecular and cellular aspects of thiol-disulfide exchange. Adv Enzymol Relat Areas Mol Biol 63, 69–172.
Hatahet F, Ruddock LW (2009). Protein disulfide isomerase: a critical evaluation of its function in disulfide bond formation. Antioxid Redox Signal 11, 2807–2850.
Holmgren A (1985). Thioredoxin. Annu Rev Biochem 54, 237–271.
Huang S, Henry L, Ho YK, Pownall HJ, Rudenko G (2010). Mechanism of LDL binding and release probed by structure-based mutagenesis of the LDL receptor. J Lipid Res 51, 297–308.
Jackson LP, Lewis M, Kent HM, Edeling MA, Evans PR, Duden R, Owen DJ (2012). Molecular basis for recognition of dilysine trafficking motifs by COPI. Dev Cell 23, 1255–1262.
Kouwen TR, Andrell J, Schrijver R, Dubois JY, Maher MJ, Iwata S, Carpenter EP, van Dijl JM (2008). Thioredoxin A active-site mutants form mixed disulfide dimers that resemble enzyme-substrate reaction intermediates. J Mol Biol 379, 520–534.
Kulak NA, Pichler G, Paron I, Nagaraj N, Mann M (2014). Minimal, encapsulated proteomic-sample processing applied to copy-number estimation in eukaryotic cells. Nat Methods 11, 319–324.
Lappi AK, Lensink MF, Alanen HI, Salo KE, Lobell M, Juffer AH, Ruddock LW (2004). A conserved arginine plays a role in the catalytic cycle of the protein disulphide isomerases. J Mol Biol 335, 283–295.
Lewis MJ, Pelham HR (1992). Ligand-induced redistribution of a human KDEL receptor from the Golgi complex to the endoplasmic reticulum. Cell 68, 353–364.
Ma W, Goldberg J (2013). Rules for the recognition of dilysine retrieval motifs by coatomer. EMBO J 32, 926–937.
Mancias JD, Goldberg J (2007). The transport signal on Sec22 for packaging into COPII-coated vesicles is a conformational epitope. Mol Cell 26, 403–414.
Mehrtash AB, Hochstrasser M (2018). Ubiquitin-dependent protein degradation at the endoplasmic reticulum and nuclear envelope. Semin Cell Dev Biol.
Miller EA, Beilharz TH, Malkus PN, Lee MC, Hamamoto S, Orci L, Schekman R (2003). Multiple cargo binding sites on the COPII subunit Sec24p ensure capture of diverse membrane proteins into transport vesicles. Cell 114, 497–509.
Moreau D, Kumar P, Wang SC, Chaumet A, Chew SY, Chevalley H, Bard F (2011). Genome-wide RNAi screens identify genes required for Ricin and PE intoxications. Dev Cell 21, 231–244.
Otte S, Barlowe C (2002). The Erv41p-Erv46p complex: multiple export signals are required in trans for COPII-dependent transport from the ER. EMBO J 21, 6095–6104.
Otte S, Belden WJ, Heidtman M, Liu J, Jensen ON, Barlowe C (2001). Erv41p and Erv46p: new components of COPII vesicles involved in transport between the ER and Golgi complex. J Cell Biol 152, 503–518.
Paroutis P, Touret N, Grinstein S (2004). The pH of the secretory pathway: measurement, determinants, regulation. Physiology (Bethesda) 19, 207–215.
Powers J, Barlowe C (1998). Transport of axl2p depends on erv14p, an ER-vesicle protein related to the Drosophila cornichon gene product. J Cell Biol 142, 1209–1222.
Sarkar G, Sommer SS (1990). The "megaprimer" method of site-directed mutagenesis. BioTechniques 8, 404–407.
Shibuya A, Margulis N, Christiano R, Walther TC, Barlowe C (2015). The Erv41-Erv46 complex serves as a retrograde receptor to retrieve escaped ER proteins. J Cell Biol 208, 197–209.
Tian G, Xiang S, Noiva R, Lennarz WJ, Schindelin H (2006). The crystal structure of yeast protein disulfide isomerase suggests cooperativity between its active sites. Cell 124, 61–73.
Vavassori S, Cortini M, Masui S, Sannino S, Anelli T, Caserta IR, Fagioli C, Mossuto MF, Fornili A, van Anken E, *et al.* (2013). A pH-regulated quality control cycle for surveillance of secretory protein assembly. Mol Cell 50, 783–792.
Wang L, Wang L, Vavassori S, Li S, Ke H, Anelli T, Degano M, Ronzoni R, Sitia R, Sun F, Wang CC (2008). Crystal structure of human ERp44 shows a dynamic functional modulation by its carboxy-terminal tail. EMBO Rep 9, 642–647.
Watanabe S, Harayama M, Kanemura S, Sitia R, Inaba K (2017). Structural basis of pH-dependent client binding by ERp44, a key regulator of protein secretion at the ER-Golgi interface. Proc Natl Acad Sci USA 114, E3224–E3232.
Welsh LM, Tong AH, Boone C, Jensen ON, Otte S (2006). Genetic and molecular interactions of the Erv41p-Erv46p complex involved in transport between the endoplasmic reticulum and Golgi complex. J Cell Sci 119, 4730–4740.
Wilson DW, Lewis MJ, Pelham HR (1993). pH-dependent binding of KDEL to its receptor in vitro. J Biol Chem 268, 7465–7468.
Wilson JD, Barlowe C (2010). Yet1p and Yet3p, the yeast homologs of BAP29 and BAP31, interact with the endoplasmic reticulum translocation apparatus and are required for inositol prototrophy. J Biol Chem 285, 18252–18261.
Winston F, Dollard C, Ricupero-Hovasse SL (1995). Construction of a set of convenient Saccharomyces cerevisiae strains that are isogenic to S288C. Yeast 11, 53–55.
Winzeler EA, Shoemaker DD, Astromoff A, Liang H, Anderson K, Andre B, Bangham R, Benito R, Boeke JD, Bussey H, *et al.* (1999). Functional characterization of the S. cerevisiae genome by gene deletion and parallel analysis. Science 285, 901–906.
Wuestehube LJ, Schekman RW (1992). Reconstitution of transport from endoplasmic reticulum to Golgi complex using endoplasmic reticulum-enriched membrane fraction from yeast. Methods Enzymol 219, 124–136.
Yang K, Li DF, Wang X, Liang J, Sitia R, Wang CC, Wang X (2016). Crystal structure of the ERp44-peroxiredoxin 4 complex reveals the molecular mechanisms of thiol-mediated protein retention. Structure 24, 1755–1765.
Yoo W, Cho EB, Kim S, Yoon JB (2019). The E3 ubiquitin ligase MARCH2 regulates ERGIC3-dependent trafficking of secretory proteins. J Biol Chem 294, 10900–10912.
Yuen CY, Wong K, Christopher DA (2016). Phylogenetic characterization and promoter expression analysis of a novel hybrid protein disulfide isomerase/cargo receptor subfamily unique to plants and chromalveolates. Mol Genet Genomics 291, 455–469.
Zimmermann L, Stephens A, Nam SZ, Rau D, Kubler J, Lozajic M, Gabler F, Soding J, Lupas AN, Alva V (2018). A completely reimplemented MPI bioinformatics toolkit with a new HHpred server at its core. J Mol Biol 430, 2237–2243.